Effects of Salt Concentration on Analyte Response Using Electrospray Ionization Mass Spectrometry

Terri L. Constantopoulos, George S. Jackson, and Christie G. Enke*

Department of Chemistry, University of New Mexico, Albuquerque, New Mexico, USA

The effect of salt concentration on analyte response using electrospray ionization mass spectrometry (ESI-MS) was measured and compared to that predicted by Enke's equilibrium partitioning model. The model predicts that analyte response will be proportional to concentration and that the response factor will decrease with increasing electrolyte concentration. The measured analyte response is proportional to concentration over four orders of magnitude when the electrolyte concentration is below 10^{-3} M, as the model predicts. The concentration of excess charge ([Q]) generated by the ESI process increases significantly at 10^{-3} M ionic concentration, but the response factor decreases at this concentration. Changes in shape of the spray that cause a loss of ion transmission efficiency may be the basis for the decrease in response. An increase in the analyte response factor with increasing electrolyte concentration is observed for electrolyte concentrations below 10^{-3} M. An explanation for this based on the electrical double layer is proposed. (J Am Soc Mass Spectrom 1999, 10, 625–634) © 1999 American Society for Mass Spectrometry

The ability of electrospray ionization (ESI) to extend the *m/z* range of mass analyzers with upper mass-to-charge limits has helped with the identification, mechanistic interpretation, and structural elucidation of biomolecules [1–3]. Furthermore, the sensitivity of the technique has increased with the introduction of nanospray [4] and microspray [5]. Despite the high level of interest in and large volume of work done with ESI, it is still very difficult to predict the effects of solvent, analyte, and electrolyte on the peak intensities in the mass spectrum. For many singly and doubly charged ions, the relative intensities of the ions in the spectrum do not reflect the relative concentrations of the ions in solution [6], sometimes by several orders of magnitude. This potentially high selectivity has limited the capabilities of ESI and avoiding matrix effects has become something of an art. However, the application of ESI could be optimized on fundamental grounds if the mechanism of selectivity is understood.

Charged droplets are created when a high voltage is applied at the tip of the ESI needle. The charged droplets move down an electric field between the needle tip and a metal plate. The resulting current is equal to the rate of charge separation occurring at the tip. Ions become desolvated by some process as they move toward the metal plate. Two mechanisms have been proposed for this process. The first is called coulomb fission. In this process the charge density eventually gets large enough to overcome the surface tension of the droplet and cause it to divide [7, 8]. Coulomb fission may cause the creation of droplets of various sizes. If the fission process creates many smaller droplets, it may be referred to as "droplet jet fission" [9]. The second mechanism, proposed by Iribarne and Thomson [10], is called ion evaporation. In this mechanism too, the charge density increases while the solvent evaporates. However, instead of forming smaller and smaller droplets, the coulombic repulsion overcomes the charged species adhesion to the surface and some ions are expelled directly from the surface. Although these proposed mechanisms do predict how ions in the ESI droplet are transferred into the gas phase, neither mechanism predicts the preferential expression of particular species in the mass spectrum.

Tang and Kebarle used Iribarne and Thomson's ion evaporation mechanism to propose a model wherein the ion evaporation rate is proportional to the concentration of the ion in the droplet [11]. They proposed the following equation:

$$I(A^+, ms) = Pf \frac{k_A[A^+]}{k_A[A^+] + k_E[E^+]} I \qquad (1)$$

to predict the mass spectrometrically detected analyte ion intensity, $I(A^+, ms)$, for a solution containing a single analyte and electrolyte where [A^+] and [E^+] are analyte and electrolyte concentrations (E^+ is due to

Address reprint requests to Dr. Christie G. Enke, Department of Chemistry, Clark Hall 103, University of New Mexico, Albuquerque, NM 87131-1096. E-mail: enke@unm.edu

impurities in the solvent), k_A and k_E are rate constants expressing the rate of transfer of analyte and electrolyte ions to the gas phase, I is the electrospray current, f is the fraction of ions converted into the gas phase, and P is a proportionality constant expressing the "sampling efficiency" of the system.

Experimentally measured response curves reveal two distinct regions. In the first region at low analyte concentrations ($[A^+] < 10^{-5}$ M) the curve is linear with a slope of ~1 on a log–log plot and $I(A^+$, ms) is proportional to $[A^+]$. The electrolyte concentration $[E^+]$ is much larger than $[A^+]$ in this region. In the second region at high analyte concentrations the curve levels off and even decreases in intensity. Here $[A^+] \gg [E^+]$. The response depends on the ratio of rate constants k_A/k_E, which is a "fractionation factor" in the ESI conversion of ions in solution to ions in the gas phase. Tang and Kebarle were unable to obtain a fit of eq 1 to experimentally measured analyte responses over a wide range of concentrations (10^{-8}–10^{-3} M) using the same k ratio [9]. A good fit was obtained with eq 1 in the low-concentration range of A^+ ($<10^{-5}$ M) with the assumption that $k_A/k_E = 1$. However, the predicted response curve deviates from the measured responses at high A^+ concentrations ($>10^{-5}$ M), indicating that the actual value of k_A/k_E is greater than one [11]. If the actual k ratio is greater than one, the fitted constant at low A^+ concentrations will be too high for experimentally measured responses in that A^+ concentration regime.

In order to address the changes in k ratios as well as the selectivity of species in the mass spectrum, Tang and Kebarle extended the model to include surface activity and ion solvation energies [9, 12]. In doing so, they also considered models for the evaporation of gas-phase ions from the droplets as well as the fission processes through which very small droplets are formed that lead to ions. This version of their model uses a depletion phenomenon to explain the decrease in k_A/k_E observed at low A^+ concentrations. Ion evaporation is assumed to occur at the surface of the droplet. Analyte ions with a higher surface activity have a higher concentration at the surface than in the bulk (ions with low ion cluster solvation energies generally have high surface activity). A higher ion evaporation constant means that A^+ ions will evaporate at a higher rate than E^+ ions. According to Tang and Kebarle, the total A^+ ions available for conversion to gas-phase ions is the sum of A^+ ions in the surface plus A^+ ions in the bulk of the droplets. Analyte ions that evaporate from the surface are thus replaced by A^+ ions from the bulk. At high A^+ concentrations, A^+ ions are rapidly supplied from the bulk as A^+ ions evaporate from the surface, maintaining a constant ratio of A^+/E^+ ions at the surface of the droplet, resulting in a higher k_A/k_E ratio. At low A^+ concentrations, all of the A^+ ions are at the surface of the droplet, where they evaporate at a high rate. Because there are no A^+ ions in the bulk to replenish those evaporated from the surface, rapid evaporation of A^+ ions leads to a depletion of A^+ ions

relative to E^+ ions at the surface of the droplet. The result is a decrease in the k_A/k_E ratio.

The surface activity and depletion phenomenon does explain why two different concentration-dependent values are observed for the k_A/k_E ratio. Surface activity also provides a means to predict why some species are preferentially expressed in the mass spectrum based on the relative concentration of analytes at the surface of the droplet. However, eq 1 is not mathematically predictive of analyte response because the effect of surface activity is not included in the equation. Furthermore, the surface activity is best applied to the determination of k_A/k_E ratios in the high-concentration region where there is no depletion. The k_A/k_E ratios determined in this region do not fit experimental data from the low-concentration region, where the surface charge ratio cannot be maintained because of depletion. Thus, the surface activity cannot be used to predict analyte response in the quantitative, low-concentration region.

Recently, Enke proposed a model to predict matrix effects based on an ion partitioning equilibrium that exists between a charged surface phase and a neutral interior phase of the ESI droplet [13]. The equilibrium partitioning model is simplistic, yet it explains much of what is observed with ESI. In many ways, this model is very similar to Tang and Kebarle's model. However, there are some fundamental differences. The equilibrium partitioning model assumes that at the instant the ESI droplet is formed there is a fixed amount, or concentration of excess charge. The remaining charges are neutralized by an equal number of counter charges and thus no new excess charge can be created during the lifetime of the droplet. Like Tang and Kebarle's model, the equilibrium partitioning model assumes that all of the excess charge will be at the surface of the droplet. However, unlike Tang and Kebarle's model, the equilibrium partitioning model defines the surface and interior of the droplet as two distinct phases between which ions (cations with positive ESI, anions with negative ESI) can partition. An equilibrium, which is defined in the next section, exists between the ions in both phases. The equilibrium partitioning constant determines which phase a given ion species will prefer based on properties of the ion including solvation energy, ion-pairing energy, charge density, and hydrophobicity of the ion as well as the nature of the counterion and the polarity of the solvent. When an ion moves to the other phase, it displaces an ion from that phase. In other words, the only way for an ion to go from the interior phase (bulk) to the surface phase is to "trade places" with an ion that is already in the surface phase. This is because no new excess charges are created after the droplet is formed.

At the time that the ESI droplet is formed, the ionic species that partition to the surface and carry the excess charge are quickly established and remain relatively unchanged throughout the evaporation process. Changes in droplet size due to evaporation do not change the absolute amount of excess ionic charge

available to be converted into the gas phase. When an ion is evaporated from the surface of the droplet, that ion is gone and cannot be replaced *as excess charge* by ions from the interior. As the ionic strength increases through desolvation, the ion properties mentioned above that favor partitioning to the surface phase only increase in magnitude. Thus, whereas it is valuable to understand the mechanism of evaporation, predictions based on the equilibrium partitioning model do not need to take into account the evaporation mechanism.

The equilibrium partitioning model differs from Tang and Kebarle's model in the equation that predicts analyte response. Equation 11, which is derived in the next section, uses the ratio of equilibrium partitioning constants (K_A/K_E) rather than the ratio of rate constants (k_A/k_E). Because the equilibrium partitioning constant is a measure of an ion's preference for the surface or interior phases, surface activity, solvation energy, hydrophobicity, and charge density (all of which affect the selectivity of ions in the mass spectrum) are each factored into this ratio. The result is that eq 11 fits experimental measurements across a wide range of concentrations (10^{-9}–10^{-3} M) with the same value of K_A/K_E.

The electrospray current is a fundamental ESI parameter, which was defined by Tang and Kebarle as the rate of excess charge production. Enke defined the concentration of excess charge, [Q], which is directly proportional to the current and inversely proportional to the flow rate [13]. The concentration of excess charge is the upper limit for the concentration of observable ions generated by the electrospray process. When analyte concentrations are less than [Q], analyte response is proportional to concentration (linear region of the response curve). When analyte concentrations are greater than [Q], saturation may occur. One advantage of knowing [Q] is that it allows the practicing mass spectrometrist to easily determine the range of quantitation for a given current and flow rate.

The equilibrium partitioning model has the potential to predict matrix effects on analyte response. This model is easy to use because it does not assume a particular evaporation mechanism and the surface activities are incorporated into the predictive equations as the partitioning constants. The partitioning constant, which is determined experimentally, is an indirect measure of the analyte properties (preference for surface or interior phase, surface activity, solvation energy, hydrophobicity, and charge density) mentioned previously for a given solvent and counterion system. Changes in solvent and/or counterion are reflected by changes in the partitioning constant. The equilibrium partitioning model is comprehensive in that it includes the effects of the ionic K values, [Q], and concentration of analyte(s) and electrolyte (all of which are easily determined experimentally) to predict analyte response. Although the equilibrium partitioning model takes a very simplistic approach, it does explain much of what is observed experimentally with ESI. The model assumes that the response of analyte ions in the mass spectrum is proportional to the concentration of analyte ions in the surface phase ($[A^+]_s$) of the initial droplet. Thus $[A^+]_s$ must be calculated in order to use the model to predict the response of a given analyte.

The Equilibrium Partitioning Model for a Single Analyte and Electrolyte

For simplicity, the following discussion is limited to positive ESI. However, the concepts also apply to negative ESI. All cations in positive ESI, including analyte and electrolyte ions, are free to partition between the surface and interior phases. For the case of a single analyte (A^+) and electrolyte (E^+), the equilibrium expressions and partitioning constants are

$$(A^+X^-)_i \rightleftharpoons (A^+)_s + (X^-)_i, \qquad K_A = \frac{[A^+]_s[X^-]_i}{[A^+X^-]_i} \tag{2}$$

$$(E^+X^-)_i \rightleftharpoons (E^+)_s + (X^-)_i, \qquad K_E = \frac{[E^+]_s[X^-]_i}{[E^+X^-]_i} \tag{3}$$

where X^- represents the counterions, and the subscripts *s* and *i* indicate surface and interior phases. Because A^+ and E^+ are both competing for a fixed number of surface charge sites, the equilibrium can be expressed as a displacement reaction

$$(A^+X^-)_i + (E^+)_s \rightleftharpoons (A^+)_s + (E^+X^-)_i \tag{4}$$
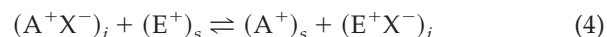
with the following partitioning constant

$$\frac{K_A}{K_E} = \frac{[A^+]_s[E^+X^-]_i}{[A^+X^-]_i[E^+]_s} \tag{5}$$

Although eq 5 can be rearranged to solve for $[A^+]_s$, it is difficult to determine $[A^+]_s$ in terms of $[A^+X^-]_i$, $[E^+X^-]_i$, and $[E^+]_s$ because these parameters are difficult to measure. The parameters $[A^+X^-]_i$, $[E^+X^-]_i$, and $[E^+]_s$ can be expressed in terms of parameters that are easily determined experimentally by introducing the concentration of excess charge, the charge balance equation, and the mass balance equation.

The concentration of excess charge [Q] is the difference in the concentrations of the cations and anions in the electrosprayed solution. The excess charge is produced at a rate that is directly proportional to the spray current (*i*) and inversely proportional to Faraday's constant (*F*). The rate of excess charge production is equal to the rate of ion production and can be expressed as the concentration of excess charge [Q] when divided by the flow rate (Γ):

$$[Q] = \frac{i}{F\Gamma} \left(\frac{\text{equivalents}}{L} \right) \tag{6}$$

The concentration of excess charge, which can easily be determined knowing the spray current and the flow

rate, is significant because it is the upper limit for observable ions generated by the electrospray process. It is also the total concentration of all ions in the surface excess charge phase, so in the case of a single analyte and electrolyte the charge balance equation is

$$[Q] = [A^+]_s + [E^+]_s \qquad (7)$$

Because the ions can exist in either the interior or the surface excess charge phases, a mass balance equation can be written for each species involved in the partitioning. For the case of a single analyte and electrolyte, the mass balance equations are

$$C_A = [A^+]_s + [A^+X^-]_i \qquad (8)$$

and

$$C_E = [E^+]_s + [E^+X^-]_i \qquad (9)$$

where C_A is the total analyte concentration and C_E is the total electrolyte concentration.

The interior concentrations ($[A^+X^-]_i$ and $[E^+X^-]_i$) in eq 5 are eliminated by substitution of eqs 8 and 9, and $[E^+]_s$ is eliminated by substitution of eq 7:

$$\begin{aligned} \frac{K_A}{K_E} &= \frac{[A^+]_s(C_E - [E^+]_s)}{(C_A - [A^+]_s)[E^+]_s} \\ &= \frac{[A^+]_s(C_E - [Q] + [A^+]_s)}{(C_A - [A^+]_s)([Q] - [A^+]_s)} \end{aligned} \qquad (10)$$

Equation 10 is quadratic in terms of $[A^+]_s$, as shown by the following rearrangement:

$$[A^+]_s^2\left(\frac{K_A}{K_E} - 1\right) - [A^+]_s\left[[Q]\left(\frac{K_A}{K_E} - 1\right)\right.$$
$$\left. + C_A\frac{K_A}{K_E} + C_E\right] + C_A[Q]\frac{K_A}{K_E} = 0 \qquad (11)$$

The analyte surface concentration $[A^+]_s$ can thus be calculated as a function of C_A, C_E, K_A/K_E, and $[Q]$, all of which can be determined experimentally (values for K_A/K_E are obtained from the ratio of intensities of A^+/E^+ in the saturation region). For values of C_A that are much lower than $[Q]$, eq 11 reduces to

$$[A^+]_s = C_A\left(\frac{K_A/K_E}{K_A/K_E - 1 + C_E/[Q]}\right) \qquad (12)$$

The response of a particular analyte ion in the mass spectrum (R_A), which is the total intensity of that analyte ion measured at the detector, can be considered in terms of the rate of ion arrival at the detector (counts), where R_A is proportional to $[A^+]_s$, the flow rate (Γ), Faraday's constant (F), transfer efficiency of

A^+ (P_A) and desolvation efficiency of A^+ (f_A) (a similar equation can be used for the electrolyte response, R_E).

$$R_A \text{ (counts)} \propto [A^+]_s\Gamma FP_A f_A\left(\frac{\text{Coulombs}}{\text{s}}\right) \qquad (13)$$

If more than one analyte peak is present due to fragmentation or analyte adducts, R_A is the sum of the intensities of all peaks attributed to the analyte ion. A detailed description of how to determine P and f is provided by Tang and Kebarle [12]. The response factor R_A/C_A is

$$\frac{R_A}{C_A} \text{ (counts)} \propto \frac{[A^+]_s\Gamma FP_A f_A}{C_A} \qquad (14)$$

When more than one analyte is present in a solution, the C_A of each analyte, C_E, K_A/K_E, and $[Q]$ have a unique effect on the response of each analyte ion. This results in the discrepancy between concentration in the solution and relative intensity in the mass spectrum. Competition between ion species (selectivity) becomes particularly severe when the total analyte concentration exceeds $[Q]$.

Response factors predicted by eq 11 of the equilibrium partitioning model are shown in Figure 1 for the case of a single analyte and electrolyte. In each of these examples it is assumed that $Pf = 1$ and thus the response, $R_A = [A^+]_s$. The effects of K_A/K_E (Figure 1a) and of C_E (Figure 1b) on $[A^+]_s$ are also predicted using eq 11. The value $[Q] = 10^{-5}$ equiv/L was used in the calculations and was determined from eq 6 for typical conditions where $\Gamma = 6$ μL/min and $i = 10^{-7}$ A. The predictions are based on the assumption that the value of $[Q]$ remains constant. When C_A is much less than $[Q]$, virtually all of the excess charge must come from electrolyte ions. Therefore, the minimum electrolyte concentration is the same as $[Q]$ and thus the value of 10^{-5} M was used for C_E. A log–log plot is used because of the need to accommodate concentrations over a range of six orders of magnitude. A slope of one on the log–log plot indicates that $[A^+]_s$ is proportional to C_A. The model predicts that when C_A is less than $[Q]$ ($C_A < 10^{-5}$ M), $[A^+]_s$ is proportional to C_A. Saturation is reached when $[A^+]_s = [Q]$. This occurs because the excess charge carried by the analyte cannot exceed the total excess charge. The C_A at which saturation occurs is a function of $[Q]$, C_E, and K_A/K_E, and can be determined by substituting $[Q]$ for $[A^+]_s$ into eq 11:

$$C_{A(\text{sat'n})} \geq \frac{[Q](K_A/K_E - 1)}{K_A/K_E} + \frac{C_E}{K_A/K_E} \qquad (15)$$

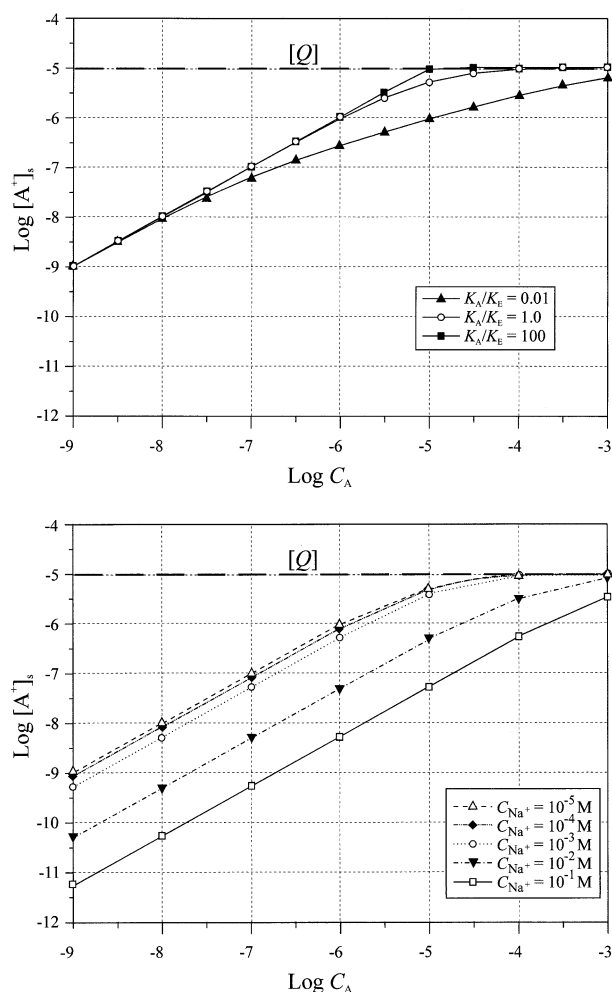When K_A/K_E is very large ($K_A/K_E \gg 1$) eq 15 simplifies to

Figure 1. (a) Effect of K_A/K_E on analyte surface concentration, $[A^+]_s$, predicted from eq 11 where K_A/K_E is increased from 0.01 to 100. C_A ranges from 10^{-9} to 10^{-3} M, $C_E = [Q] = 10^{-5}$ M. An effect of changing K_A/K_E predicted by the model is the change in degree of rounding of the response curve between the linear and saturation regions. (b) Effect of C_E on analyte surface concentration, $[A^+]_s$, predicted from eq 11 where C_E ranges from 10^{-5} to 10^{-1} M and is constant for each series. C_A ranges from 10^{-9} to 10^{-3} M. $[Q] = 10^{-5}$ M and $K_A/K_E = 50$. The model predicts that a smaller fraction of the analyte ions are part of the surface excess charge when C_E exceeds $[Q]$, indicating a decrease in ionization efficiency. The model also predicts that saturation occurs at higher C_A when C_E exceeds $[Q]$.

$$C_{A(sat'n)} \geq [Q] + \frac{C_E}{K_A/K_E} \qquad (16)$$

Figure 1a shows the effect of K_A/K_E on $[A^+]_s$ predicted by eq 11. K_A/K_E is unitless and ranges from 0.01 to 100. When $C_A \ll [Q]$, essentially all of the analyte ions are part of the surface excess charge and $[A^+]_s$ is proportional to C_A. This is true regardless of the value of K_A/K_E. One of the effects of various values of K_A/K_E is the degree of rounding in the response curve between the low-concentration region and the saturation region at higher concentrations. For values of K_A/K_E greater than one, the linear portion of the curve approaches

$[Q]$. This is a very favorable operating condition because $[A^+]_s$ is maximized for values of C_A approaching saturation.

Figure 1b shows the effect of C_E on $[A^+]_s$ predicted by eq 11. A constant value of 50 was used for K_A/K_E. When $C_E = [Q]$ and $C_A \ll [Q]$, essentially all of the analyte ions are part of the surface excess charge and $[A^+]_s$ is proportional to C_A. The model predicts that when C_E exceeds $[Q]$, a smaller fraction of the analyte ions are part of the surface excess charge ($[A^+]_s < C_A$). $[A^+]_s$ is still proportional to C_A, but the ionization efficiency is decreased. This effect becomes more pronounced as C_E increases, as shown in Figure 1b. Another effect observed when C_E exceeds $[Q]$ is that $[A^+]_s = [Q]$ (saturation) occurs at higher C_A.

The equilibrium partitioning model can be used to predict the effects of the ionic K values, $[Q]$, and concentration of analyte(s) and electrolyte (all of which are easily determined experimentally) on analyte response (R_A). This study focuses on the effect of electrolyte concentration, C_E on analyte response. Analyte responses have been measured at several electrolyte concentrations and compared to the values of $[A^+]_s$ predicted by the model using experimental parameters.

Experimental

All ESI-MS experiments were conducted using a Finnigan MAT Triple Stage Quadrupole (TSQ) 7000 mass spectrometer with a modified Finnigan API source (San Jose, CA). The standard Finnigan API needle assembly was replaced with a World Precision Instruments model TAURUS-R X-Y-Z Micromanipulator (Sarasota, FL), to which the ESI needle is mounted. The sample was introduced into the ESI needle from a 250 μL gas tight syringe using a Harvard Apparatus Model 22 syringe pump (South Natick, MA). The sample was pumped into the metal ESI needle through a 100 μm i.d. fused silica capillary at a flow rate of 8 μL/min. The syringe was connected to the 100 μm i.d. capillary via a 250 μm i.d. fused silica capillary transfer line. A potential of 2.5 kV was applied through direct electrical contact with the metal needle. In order to obtain accurate measurements of the spray current, a digital voltmeter was added in series with the electrospray needle. The voltmeter was converted into a current meter by adding two shunt resistors, along with a sliding switch, which enabled us to measure the current on two scales: 0–199 nA and 0–1999 nA. The ions were mass analyzed by scanning with the third quadrupole of the TSQ 7000 across a mass range of m/z 0–500. Spectra were acquired by recording and summing multiple scans using Finnigan MAT ICIS software version 8.1.1 as the instrument data system. Several summed spectra were averaged for each concentration.

A stock solution of 10^{-2} M sodium chloride (NaCl, Columbus Chemical Industries, Columbus, WI) was prepared by dissolving NaCl in a few drops of purified water, then diluting to volume with B&J Brand pure

methanol (Burdick & Jackson, Muskegon, MI). Four more stock solutions of NaCl ranging in concentration from 10^{-3} to 10^{-6} M were prepared by conducting several 10-fold dilutions of the 10^{-2} M NaCl solution with methanol. Stock solutions of 10^{-2} M tetrapentylammonium bromide (TPABr, Aldrich Chemical, St. Louis, MO) were prepared by dissolving TPABr in a portion of each stock NaCl solution. Finally, several 10-fold dilutions of each stock TPABr solution were conducted using the appropriate stock NaCl solution as the solvent to prepare a series of TPABr solutions ranging in concentration from 10^{-3} to 10^{-9} M for each NaCl concentration.

The effects of salt concentration on analyte response were determined experimentally using the tetrapentylammonium ion (TPA^+) as the analyte, the sodium ion (Na^+) as the electrolyte, and methanol as the solvent. In all experiments the analyte concentration (C_{TPA^+}) ranged from 10^{-9} to 10^{-3} M and the electrolyte concentration (C_{Na^+}) ranged from 10^{-6} to 10^{-3} M (C_{Na^+} was constant for each series of C_{TPA^+}). [Q] was determined using eq 6 where $\Gamma = 8$ μL/min and i is the electrospray current measured at each C_{TPA^+} and C_{Na^+}.

Results and Discussion

Comparison of Predicted and Measured Salt Concentration Effects on TPA^+ Response

The effect of salt concentration on the surface concentration of TPA^+ ($[TPA^+]_s$) was predicted using eq 11 with actual experimental parameters and compared to the measured analyte response (R_{TPA^+}). Values for the ratio K_A/K_E, which were obtained from the ratio of intensities of TPA^+/Na^+ in the saturation region, range from 24 to 106. The difference of less than one order of magnitude in the values of K_{TPA^+}/K_{Na^+} has little effect on $[TPA^+]_s$, therefore the value $K_{TPA^+}/K_{Na^+} = 50$ was selected for the calculations because it is near the center of the range. It is worth pointing out that in the low-concentration region the value of the ratio of TPA^+ and Na^+ responses is 9.61. This value is within experimental error of the value of $k_{TPA^+}/k_{Na^+} = 8.75$, the ratio of the rate constants (k) reported by Kebarle and Tang [14] for this same region.

The equilibrium partition model predicts that the response factor ($[TPA^+]_s\Gamma FP_{TPA^+}f_{TPA^+}/C_{TPA^+}$) will have a slope of one on a log–log plot at low analyte concentration (C_{TPA^+}) and will approach saturation when $C_{TPA^+} = 10^{-4}$ M if $P_{TPA^+}f_{TPA^+}$ remains constant over the range of experimental conditions (Figure 2a). The model also predicts that the response factor will decrease as electrolyte concentration (C_{Na^+}) increases. The experimental data in Figure 2b reveals that when $C_{Na^+} < 10^{-3}$ M the measured TPA^+ response factor has a slope of one on a log–log plot over four orders of magnitude at low C_{TPA^+} and approaches saturation when $C_{TPA^+} = 10^{-4}$ M, as predicted by the model. This confirms the prediction that response is proportional to
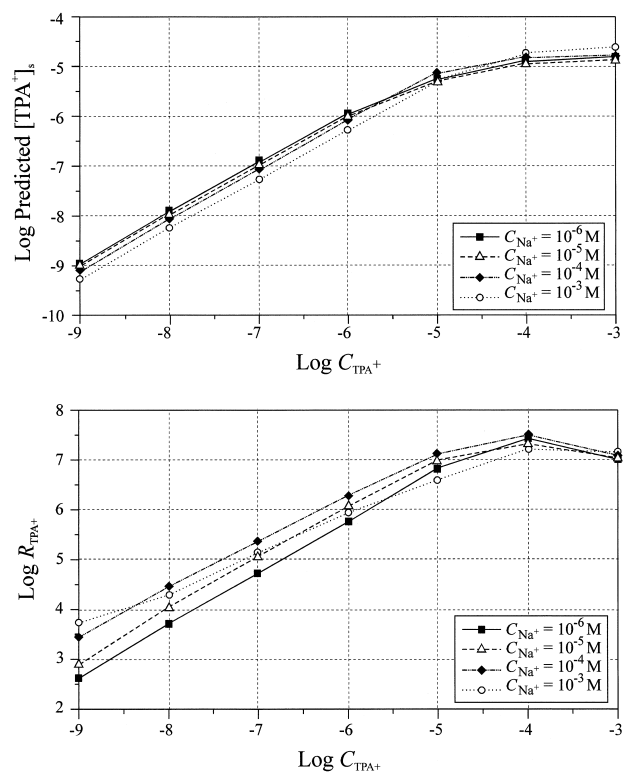

Figure 2. (a) Effect of C_{TPA^+} and C_{Na^+} on $[TPA^+]_s$ predicted from eq 11 using experimental parameters. [Q] was calculated from eq 6 using the measured i for each concentration and $\Gamma = 8$ μL/min. C_{TPA^+} ranges from 10^{-9} to 10^{-3} M. C_{Na^+} ranges from 10^{-6} to 10^{-3} M and is constant for each series, $K_A/K_E = 50$. The model predicts a slope of one on a log–log plot at low C_{TPA^+} and saturation when $C_{TPA^+} = 10^{-4}$ M. The model also predicts that the response factor will decrease as C_{Na^+} increases. (b) Effect of C_{TPA^+} and C_{Na^+} on measured R_{TPA^+}. C_{TPA^+} ranges from 10^{-9} to 10^{-3} M. C_{Na^+} ranges from 10^{-6} to 10^{-3} M and is constant for each series. A slope of one on a log–log plot over four orders of magnitude at low C_{TPA^+} and saturation when $C_{TPA^+} = 10^{-4}$ M is observed, as predicted by the model. An *increase* in R_{TPA^+} is observed as C_{Na^+} increases to 10^{-4} M, contrary to the predictions of the model. R_{TPA^+} decreases when $C_{TPA^+} + C_{Na^+} = 10^{-3}$ M.

concentration at low C_A. However, contrary to the predictions of the model, Figure 2b reveals that R_{TPA^+} *increases* as C_E increases when $C_{Na^+} < 10^{-3}$ M. Also, the measured TPA^+ response decreases in the saturation region ($C_{TPA^+} = 10^{-3}$ M). Furthermore, at still higher Na^+ concentrations ($C_{Na^+} = 10^{-3}$ M), R_{TPA^+} decreases. These differences between the measured response and the predicted surface concentration of analyte caused us to more carefully examine the effects of salt concentration on the analyte response.

Effect of Salt Concentration on [Q]

Assuming that the response of all species is proportional to [Q], it is important to understand how [Q] depends on the concentration of salt in the electrospray solution. The effects of both C_{Na^+} and C_{TPA^+} on [Q] are shown in Figure 3. The minimum value of [Q] is measured in "pure" methanol solvent, which has a
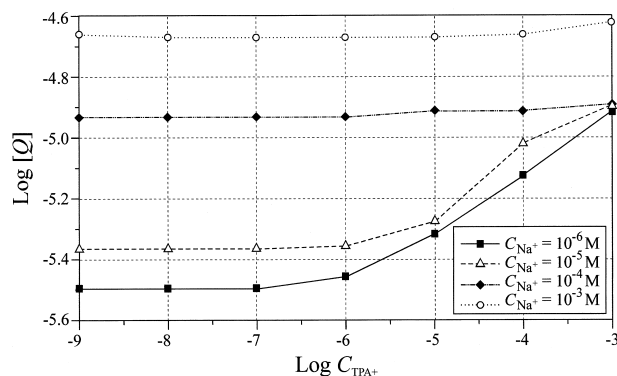
Figure 3. Effect of C_{TPA^+} and C_{Na^+} on $[Q]$. $[Q]$ was calculated from eq 6 using the measured i for each concentration and $\Gamma = 8$ μL/min. C_{TPA^+} ranges from 10^{-9} to 10^{-3} M. C_{Na^+} ranges from 10^{-6} to 10^{-3} M and is constant for each series. The minimum value of $[Q]$ (C_{Na^+} of 10^{-6} M) is measured in "pure" methanol solvent. Increasing C_{Na^+} increases $[Q]$ as well as the minimum value of $[Q]$ for a given TPA$^+$ series. When C_{TPA^+} is less than C_{Na^+}, C_{TPA^+} has no effect on $[Q]$. When $C_{TPA^+} \geq C_{Na^+}$, $[Q]$ increases with C_{TPA^+}. $[Q]$ is larger for a given C_{Na^+} than it is for the same C_{TPA^+} which is attributed to the higher conductivity of Na$^+$.

background C_{Na^+} of 10^{-6} M [14, 15]. Increasing C_{Na^+} increases not only $[Q]$, but also the minimum value of $[Q]$ that occurs in a given TPA$^+$ series. It is worth noting that an increase of three orders of magnitude in C_{Na^+} corresponds to an increase of only one order of magnitude in $[Q]_{min}$. When C_{TPA^+} is less than C_{Na^+}, $[Q]$ is carried by Na$^+$ so that C_{TPA^+} has no effect on $[Q]$. When $C_{TPA^+} \geq C_{Na^+}$, $[Q]$ is carried by TPA$^+$ and increases with C_{TPA^+}. This behavior has been observed by others and reported in terms of the spray current [14, 16, 17]. Increases in $[Q]$ with salt concentration at constant flow rate are expected. This is caused by an increase in the spray current, which is a function of the conductivity of the solution [11].

In general, $[Q]$ is larger for a given C_{Na^+} than it is for the same C_{TPA^+}. Values of $[Q]$ are approximately the same at 10^{-3} M TPA$^+$ when $C_{Na^+} < 10^{-3}$ M. The value of $[Q]$ is larger when $C_{Na^+} = 10^{-3}$ M. This effect is attributed to the higher conductivity of Na$^+$.

Effect of Salt Concentration on Total Response

The total response (R_{total}) is the sum of intensities of all TPA$^+$ and Na$^+$ peaks ($R_{TPA^+} + R_{Na^+}$). A plot of R_{TPA^+}, R_{Na^+}, and R_{total} is shown in Figure 4 for the series with $C_{Na^+} = 10^{-4}$ M. In general, when C_{TPA^+} is less than C_{Na^+}, R_{total} is constant and is dominated by C_{Na^+}. When $C_{TPA^+} \geq C_{Na^+}$, R_{total} is dominated by C_{TPA^+}. Increasing C_{TPA^+} increases both the total salt concentration and R_{total}.

If R_{total} were proportional to $[Q]$, then we would expect to see the same trends in total response as those seen in $[Q]$ when plotted as a function of salt concentration. The effects of both C_{Na^+} and C_{TPA^+} on R_{total} are shown in Figure 5. Comparison to Figure 3 shows that in general, the trends are the same. Total response and
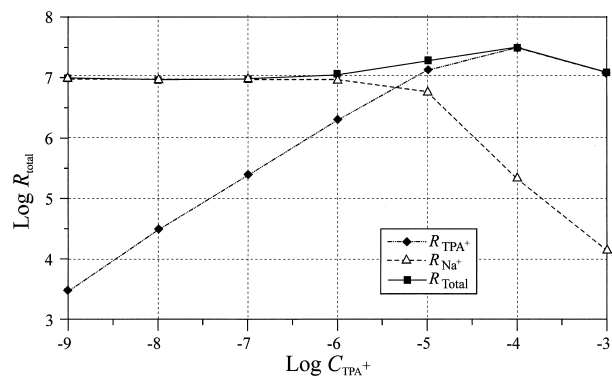

Figure 4. Effect of C_{TPA^+} on R_{TPA^+}, R_{Na^+}, and R_{total} at constant C_{Na^+}. C_{TPA^+} ranges from 10^{-9} to 10^{-3} M. $C_{Na^+} = 10^{-4}$ M. When C_{TPA^+} is less than C_{Na^+}, R_{total} is constant and is dominated by C_{Na^+}. When $C_{TPA^+} \geq C_{Na^+}$, R_{total} is dominated by C_{TPA^+}. Increasing C_{TPA^+} increases both the total salt concentration and R_{total}.

$[Q]$ both increase with increasing C_{Na^+}. When C_{TPA^+} is less than C_{Na^+}, R_{total} and $[Q]$ are both constant. When $C_{TPA^+} \geq C_{Na^+}$, R_{total} and $[Q]$ both increase. Although these trends are the same, the plots do differ in their relative increases as a function of C_{Na^+}. For example, when C_{Na^+} is increased from 10^{-4} to 10^{-5} M a smaller increase in $[Q]$ corresponds to a larger increase in R_{total} than when C_{Na^+} is increased from 10^{-5} to 10^{-4} M.

At high salt concentrations, changes in $[Q]$ no longer correspond to changes in R_{total}. When C_{Na^+} increases from 10^{-4} to 10^{-3} M, $[Q]$ increases as expected. However R_{total} decreases. A decrease in R_{total} is also seen as C_{TPA^+} approaches 10^{-3} M for every C_{Na^+} series. This is consistent with the TPA$^+$ response that was observed in Figure 2b when $C_{TPA^+} = 10^{-3}$ M. These differences reveal that the efficiency of the conversion of $[Q]$, the excess charge, to measurable ions is lower at the highest
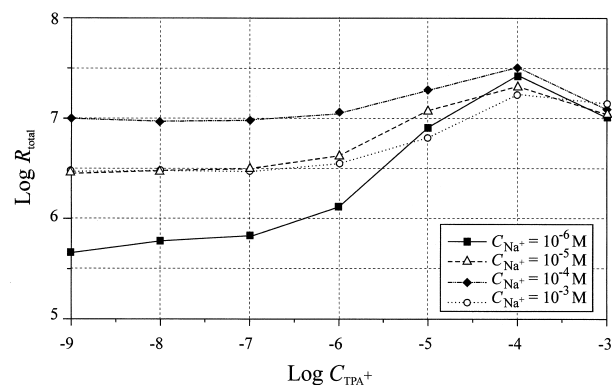

Figure 5. Effect of C_{Na^+} and C_{TPA^+} on R_{total}. C_{TPA^+} ranges from 10^{-9} to 10^{-3} M. C_{Na^+} ranges from 10^{-6} to 10^{-3} M and is constant for each series. Trends in total response are similar to $[Q]$ (Figure 3): R_{total} increases with increasing C_{Na^+}, is constant when C_{TPA^+} is less than C_{Na^+}, and increases when $C_{TPA^+} \geq C_{Na^+}$. Figures 3 and 5 differ in the relative increases as a function of C_{Na^+}. At high salt concentrations, changes in $[Q]$ (Figure 3) no longer correspond to changes in R_{total}, indicating that the conversion of $[Q]$ to measurable ions is less efficient at the highest salt concentrations.
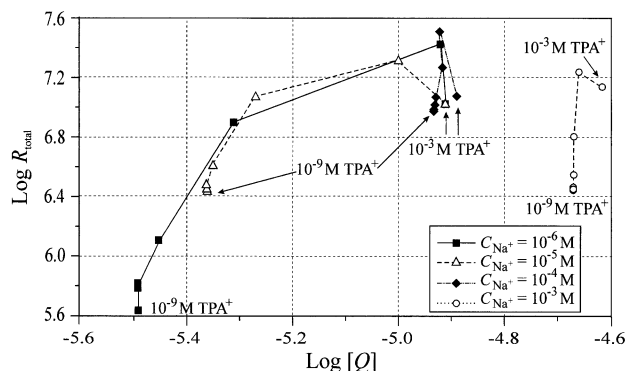
Figure 6. Effect of C_{Na^+}, C_{TPA^+}, and $[Q]$ on R_{total}. C_{TPA^+} ranges from 10^{-9} to 10^{-3} M and increases to the right for each series. C_{Na^+} ranges from 10^{-6} to 10^{-3} M and is constant for each series. $[Q]$ was calculated from eq 6 using the measured i for each concentration and $\Gamma = 8$ μL/min. Changes in R_{total} are not proportional to changes in $[Q]$. Small increases in R_{total} at low C_{TPA^+}, where $[Q]$ is constant, reflect the increases observed in R_{TPA^+} at those concentrations (see Figure 2b). Increases in R_{total} correspond to increases in $[Q]$ when $C_{TPA^+} \geq C_{Na^+}$. A decrease in R_{total} corresponds to an increase in $[Q]$ when $C_{TPA^+} = 10^{-3}$ M, indicating that a smaller fraction of those ions reach the detector.

salt concentrations than it is at lower salt concentrations.

Effect of [Q] on Total Response

In general, both $[Q]$ and R_{total} have been shown to increase with increasing salt concentration. If desolvation and ion transfer efficiencies are constant, increases in R_{total} should be proportional to increases in $[Q]$. Figure 6 shows R_{total} plotted as a function of $[Q]$, with C_{TPA^+} increasing toward the right for each series. Changes in R_{total} are clearly not proportional to changes in $[Q]$. At low C_{TPA^+}, where $[Q]$ is constant, small increases observed in R_{total} reflect the increases observed in R_{TPA^+} at those concentrations (Figure 2b). When $C_{TPA^+} \geq C_{Na^+}$, increases in R_{total} correspond to increases in $[Q]$. At the lower Na^+ concentrations ($C_{Na^+} < 10^{-4}$ M), increasing C_{TPA^+} from 10^{-6} to 10^{-5} M results in a relatively large increase in R_{total} compared to the increase in $[Q]$. If R_{total} were proportional to $[Q]$, increasing C_{TPA^+} from 10^{-5} to 10^{-4} M would have resulted in a much larger increase in R_{total} corresponding to the large increase in $[Q]$. Instead, there is a relatively small increase in R_{total}. Finally, increasing C_{TPA^+} to 10^{-3} M results in a decrease in R_{total} that corresponds to an increase in $[Q]$. This indicates that although there is a larger concentration of excess charge at high salt concentrations, a smaller fraction of those ions reach the detector. The change in slope when C_{TPA^+} is increased to 10^{-4} M suggests a reduction in ion transfer efficiency at concentrations above 10^{-5} M that becomes more drastic at 10^{-3} M. It is interesting to note that the range in values of $[Q]$ decreases for each series as C_{Na^+} increases. This is because increasing C_{Na^+} increases the minimum value of $[Q]$, thus reducing the range between minimum and maximum.
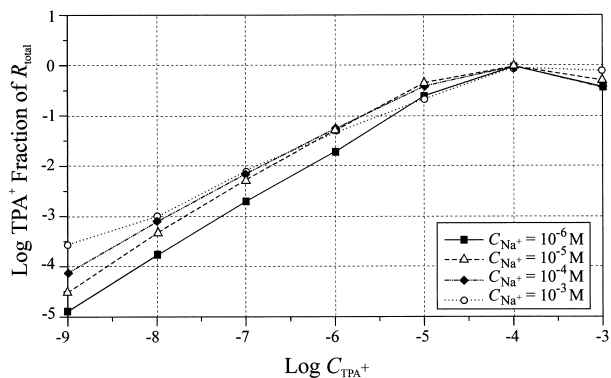

Figure 7. R_{TPA^+} is plotted as its fraction of R_{total} to determine if there is a relative decrease in R_{TPA^+} (with respect to R_{total}) with increasing C_{Na^+}, as the model predicts. An increase in the fraction of R_{total} is observed with increasing C_{Na^+}, indicating that R_{TPA^+} does increase increasing C_{Na^+}.

Effect of Salt Concentration on Fraction of Analyte Response

Although the model predicts that the TPA^+ response will decrease with increasing C_{Na^+}, Figure 2b shows that the TPA^+ response increases instead. Perhaps the increase observed in R_{TPA^+} is due to the increase observed R_{total} with increasing C_{Na^+} (Figure 5). If this is true, then a plot of R_{TPA^+} as its fraction of R_{total} would show a relative decrease in R_{TPA^+} with increasing C_{Na^+}. Such a plot is shown in Figure 7, and to the contrary, an increase in R_{TPA^+} is observed with increasing C_{Na^+}.

Conclusions

The measured TPA^+ response is proportional to concentration over four orders of magnitude at low C_{TPA^+}, as predicted by the equilibrium partitioning model (Figure 2). An unexpected decrease in both R_{TPA^+} and R_{total} occurs at the highest salt concentrations (10^{-3} M). The measured TPA^+ response, R_{TPA^+}, increases with increasing C_{Na^+}, which is contrary to the prediction that R_{TPA^+} would be suppressed by increasing electrolyte concentration. The same effects were observed when tetrabutylammonium ion was used as the analyte and cesium ion was used as the electrolyte. These discrepancies between the observed response, R_{TPA^+}, and the predicted concentration of ions in the surface excess charge phase, $[TPA^+]_s$, need to be addressed. In this study, we have demonstrated that most of the deviations are due to the fact that ion desolvation and/or transmission are significantly decreased at the highest salt concentrations.

The fact that R_{TPA^+} and R_{total} do not follow increases in $[Q]$ and that both decrease at the highest salt concentrations (10^{-3} M) indicates that a smaller fraction of the ions reach the detector than at lower salt concentrations. The increased current that we observed at the highest salt concentrations indicates that more excess charge ions are produced in the solution phase. Thus

the decrease in response indicates a loss in ion transfer efficiency or desolvation efficiency (or both). The key may lie in the observation that changes occur in the shape of the spray as a function of salt concentration. A visible increase in the diameter of the spray was observed at high salt concentrations. This is consistent with the fact that the increase in charge density at high salt concentrations results in repulsive forces that cause the ions to spread out more. The increase in spray diameter reduces the density of ions at the center of the spray and thus fewer ions enter the mass spectrometer causing the decrease in response [18]. Further work on the deviation from the expected response at high salt concentrations may yield a proportionality factor that would compensate for the loss of ions entering the mass spectrometer. On the other hand, this may not be necessary because this problem occurs outside of the range of quantitation.

The increase in R_{TPA^+} with increasing C_{Na^+} suggests that the model may be oversimplified for these conditions. The model assumes that all of the excess charge is at the surface of the ESI droplet. However, the lower R_{TPA^+} at lower C_{Na^+} may indicate that some of the excess charge is in the interior of the droplet and is therefore more difficult to desolvate. It is useful to consider this in terms of the effects of ionic strength on the electrical double layer. When a solution is in contact with an electrode, a fixed layer of ions with charge opposite to that of the electrode forms at the boundary between the solution and the electrode (compact layer). Next to that is a diffuse layer in which the ions are free to move (diffuse layer) [19]. These two layers comprise the electrical double layer. The fraction of the excess charge within each layer depends on the ionic strength of the solution. At low ionic strength (low salt concentration) the ions comprising the excess charge are spread across both layers and thus only a fraction of the excess charge is within the compact layer. Conversely, at high enough ionic strength virtually all the excess charge is within the compact layer.

If a conducting sphere is charged, the ions carrying the excess charge spread out along the surface generating an electrical double layer with the compact layer at the surface and the adjacent diffuse layer toward the interior. In the case of a spherical conductor, the surface is in contact with air, rather than an electrode. Ions in the compact layer are not confined in the solution by a solid surface, as they are when in contact with an electrode. This allows ions with large enough positive solvation energies to "sit" on the surface of the sphere. As a result, ions in the compact layer may be only partially solvated. The partitioning constant for a particular ion between the surface and the interior of the droplet depends on its solvation energy and its ion-pair formation constant with the counterion. Ions with positive solvation energies for which it is energetically favorable to be desolvated will prefer to be on the surface where they can be only partially solvated. Ions with negative solvation energies for which it is energet-
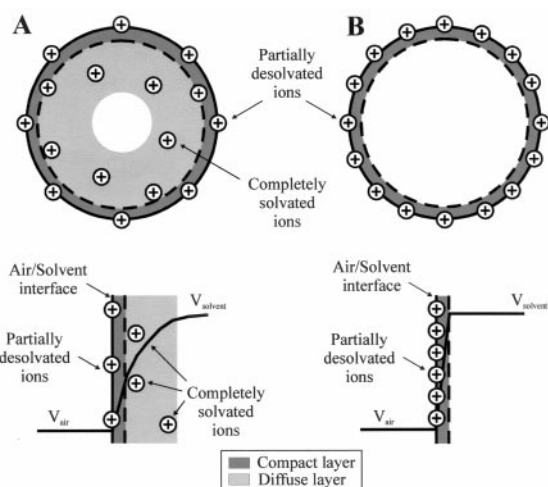

Figure 8. Effect of ionic strength on electrical double layer. Charges are within compact and diffuse layers and potential profile at the air/solvent interface. At low salt concentration (**a**) excess charge ions extend into the diffuse layer toward the interior of the droplet leaving fewer ions in the compact layer. At high salt concentration (**b**) a higher fraction of the excess charge ions are in the compact layer. Ions at the surface can be partially desolvated, ions away from the surface are completely solvated.

ically favorable to be solvated will prefer to be away from the surface where they can be completely solvated. TPA^+, which has a lower solvation energy than Na^+, is enriched on the surface due to its hydrophobic groups. Furthermore, ions with higher ion-pair formation constants will prefer to be in the solvent with the counter-charge ions.

Changes in the fraction of ions in the compact layer as a function of salt concentration, and hence ionic strength may account for the increase in R_{TPA^+} with increasing C_{Na^+}. Figure 8a shows that at low salt concentration, excess charge ions extend into the diffuse layer toward the interior of the droplet leaving fewer ions in the compact layer. A significant fraction of the excess charge ions will be solvated, thus reducing the response by reducing the fraction of the ions that are readily freed into the gas phase and detected by the mass spectrometer. Furthermore, the solvation energy is not a factor in whether or not these ions carry the excess charge. Increasing the salt concentration increases the fraction of the excess charge ions that are in the compact layer (Figure 8b). A smaller fraction of excess charge ions will be solvated, thus the response for those ions with higher solvation energy will be increased. Their electrical double layer effect could therefore account for the increase in R_{TPA^+} that was observed with increasing C_{Na^+}.

The extent of the electrical double layer effect at high ionic strength will depend on the solvation energy of the ions. Excess charge ions with negative solvation energies are more readily solvated and prefer to be away from the surface. At higher ionic strength those ions are "pushed" out toward the surface, making the electrical double layer effect more pronounced. Excess charge ions with positive

solvation energies are more solvophobic and therefore are already at the surface, making the electrical double layer effect less pronounced.

An alternative explanation could be that the increase in R_{TPA^+} with increasing C_{Na^+} is due to the decrease in droplet size with increasing conductivity of the solution [20]. De La Mora found that a 1000-fold increase in conductivity reduces the droplet size by a factor of 10. Desolvation of smaller droplets is more efficient, which may produce ions more efficiently. It could also turn out that that the increase in R_{TPA^+} with increasing C_{Na^+} is due to effects of the electrical double layer combined with the effect of increasing conductivity.

Acknowledgments

References

1. Loo, J. A.; Loo, R. O. In *Electrospray Ionization Mass Spectrometry*; Cole, R. B., Ed.; Wiley: New York, 1997; pp 385–420.

2. Crain, P. F. In *Electrospray Ionization Mass Spectrometry*; Cole, R. B., Ed.; Wiley: New York, 1997; pp 421–548.

3. Ohasi, Y. In *Electrospray Ionization Mass Spectrometry*; Cole, R. B., Ed.; Wiley: New York, 1997; pp 459–498.

4. Wilm, M.; Mann, M. *Int. J. Mass Spectrom. Ion Processes* **1994,** *136,* 167–180.

5. Emmett, M. R.; Caprioli, R. M. *J. Am. Soc. Mass Spectrom.* **1994,** *5,* 605–613.

6. Cheng, Z. L.; Siu, K. W. M.; Guevrement, R.; Berman, S. S. *J. Am. Soc. Mass Spectrom.* **1992,** *3,* 281.

7. Gomez, A.; Tang, K. *Phys. Fluids* **1994,** *6,* 404.

8. Dole, M.; Mack, L. L.; Hines, R. L.; Mobley, R. C.; Ferguson, L. D.; Alice, M. B. *J. Chem. Phys.* **1968,** *49,* 2240–2249.

9. Kebarle, P.; Ho, Y. In *Electrospray Ionization Mass Spectrometry*; Cole, R. B., Ed.; Wiley: New York, 1997; pp 3–64.

10. Iribarne, J. V.; Thompson, B. A. *J. Chem. Phys.* **1976,** *64,* 2287–2294.

11. Tang, L.; Kebarle, P. *Anal. Chem.* **1991,** *63,* 2709–2715.

12. Tang, L.; Kebarle, P. *Anal. Chem.* **1993,** *65,* 3654–3668.

13. Enke, C. G. *Anal. Chem.* **1997,** *69,* 4885–4893.

14. Kebarle, P.; Tang, L. *Anal. Chem.* **1993,** *65,* 972A–985A.

15. Constantopoulos, T. L.; Jackson, G. S.; Enke, C. G. *Anal. Chim. Acta,* to be published.

16. Ikonomou, I. G.; Blades, A. T.; Kebarle, P. *Anal. Chem.* **1991,** *63,* 1989–1998.

17. Smith, R. D.; Wahl, J. H.; Goodlett, D. R.; Hofstadler, J. A. *Anal. Chem.* **1993,** *65,* 574 A–584 A.

18. Constantopoulos, T. L.; Enke, C. G. *J. Am. Soc. Mass Spectrom,* in preparation.

19. Bard, A. J.; Faulkner, L. R. *Electrochemical Methods*; Wiley: New York, 1980.

20. Fernandez De La Mora, J. F.; Loscertales, I. G. *J. Fluid Mech.* **1994,** *260,* 155–184.